# Interferometric tracking of optically trapped probes behind structured surfaces: a phase correction method

Peter C. Seitz, Ernst H. K. Stelzer, and Alexander Rohrbach

We investigate the influence of an additional scatterer on the tracking signal of an optically trapped particle. The three-dimensional particle position is recorded interferometrically with nanometer precision by using a quadrant photodiode in the back focal plane of a detection lens. A phase disturbance underneath the sample leads to incorrect position signals. The resulting interaction potential and forces are therefore erroneous as well. We present a procedure to correct for the disturbance by measuring its interferometric signal. We prove the applicability of our phase correction approach by generating a defined displacement of the trapped probe. © 2006 Optical Society of America

*OCIS codes:* 120.5050, 140.7010, 180.3170, 290.0290, 290.5850.

## 1. Introduction

Scanning of structured surfaces can be accomplished by a multitude of techniques. In addition to mechanical probing techniques such as atomic force microscopy[1] (AFM)—which offers very high resolution in surface imaging—optical probing techniques are broadly used also in everyday life. Popular examples are data reading and storage with compact disks (CD), digital versatile disks (DVDs), or bar-code scanners. However, point or line scanning becomes more complicated in an environment with inhomogeneous refractive indices, in which absorption and phase shifts alter the optical wave and complicate the information transfer during reading and writing. This effect is already present in multilayer optical disks,[2] in which the index change at the first layer changes the optical focus that is used for reading and writing at the second layer. Arising phase disturbances due to index inhomogeneities or turbulences are well known also in optical microscopy and astronomy and can be compensated for in certain cases with adaptive optics to increase resolution and contrast.[3,4] Other microscopy techniques use white light to scan in strongly scattering environments and measure interference signals only in the focal region due to the short coherence length of the light.[5] However, in imaging applications in which laser light with long coherence lengths is advantageous, an inhomogeneous environment around the focus shifts the phase and produces additional interference effects. This influences image quality in microscopy[6] but also plays a major role in optical trapping and tracking.[7,8] Whereas the optical trapping potential is less influenced by the phase disturbance induced by a structured surface, the position detection of a trapped probe with back focal plane interferometry is strongly affected. Especially for surface scanning with trapped probes,[9–12] the influence of the surface structure (the sample) usually cannot be neglected.

Using optical tweezers based systems, interesting and challenging applications are to scan either a surface structured with immobilized proteins (e.g., via gold dots or function maintaining tags),[13,14] or even the membrane of a living cell[15] (see also Fig. 1). The interaction of proteins with binding partners is a complex mechanism both in terms of biochemistry and physics. When held in an optical trap near the coverslip, a ligand coated spherical probe (e.g., a submicrometer-sized bead) undergoes position and orientation fluctuations on a broad dynamic range, which is determined mainly by the thermodynamics of the local environment. In other words, the probe with the ligands figures out the best interaction condition within a broad range of

P. C. Seitz (p.seitz@gmx.net) and E. H. K. Stelzer are with the European Molecular Biology Laboratory, Meyerhofstrasse 1, D-69117 Heidelberg, Germany. A. Rohrbach (Rohrbach@imtek.de) is with the Laboratory for Optical Measurement Technology, Department of Microsystems Engineering (IMTEK), University of Freiburg, Georges-Köhler-Allee 102, 79110 Freiburg, Germany.
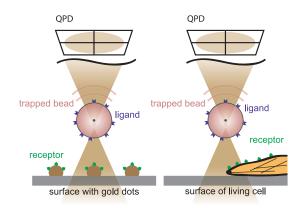
Fig. 1.   (Color online) Ligand coated spherical bead is placed near a receptor-coated surface with an optical trap. The surface structure, e.g., gold dots or a cell, disturbs the phase of the trapping laser.

distances, speeds, and orientations relative to the protein-coated surface. By recording and analyzing the change in the probe's position fluctuations, the interaction can be derived with high spatial resolution and within a broad dynamic range.[16,17] No labeling (e.g., with fluorophores) is required, since the probe's fluctuations are recorded interferometrically. The technique of optical trapping and tracking applied is called photonic force microscopy.[18] With this technique it should be possible to extend interaction experiments from the single molecule level to the screening of protein arrays.

Although the idea of scanning a surface with a trapped particle is not new,[9–12] there has been no study considering the phase changes induced by the surface structure, which can lead to significantly wrong position tracking and therefore to wrong interaction measurements. In this study we investigate the optical effects of defined surface relief structures on the tracking quality of a trapped particle, which is scanned across the structure. We propose a scheme to correct for the phase disturbance induced by the surface structure, and we prove its validity by a defined probe displacement.

## 2.  Theory

The optical trapping potential $W_{\text{trap}}(\mathbf{b})$ formed by a strongly focused laser beam and a dielectric particle is harmonic around the equilibrium position $\mathbf{b}_0$, which is located slightly behind the center of the focus. The trapping force $\partial_i W_{\text{trap}}[b_i(t)] = -\kappa_i[b_i(t) - b_{0i}]$ is linear to the displacement $\Delta b_i(t) = b_i(t) - b_{0i}$ in all dimensions $i = x, y, z$; $\partial_i = \partial/(\partial x_i)$. The trap stiffness $\kappa_i$ is related to the autocorrelation time $\tau_i$ as $\tau_i = \gamma/\kappa_i$ via the viscous drag $\gamma$. The autocorrelation time $\tau_i$ is used to calibrate the trap by using the Langevin method.[18]

Any external interaction $W_{\text{ext}}$ changes the total potential $W_{\text{tot}}$ and influences the position trace $\mathbf{b}(t)$. In thermal equilibrium, the total potential can be derived from the position distribution function $p(\mathbf{b})$ by using the Boltzmann relation

$$W_{\text{tot}}(\mathbf{b}) = -k_b T \ln(p(\mathbf{b})/p_0) = W_{\text{trap}}(\mathbf{b}) + W_{\text{ext}}(\mathbf{b}). \quad (1)$$

$p_0$ normalizes $p(\mathbf{b})$ to a probability density function, $k_b$ is the Boltzmann constant, and $T$ is the temperature of the system. From Eq. (1) the external force can be determined by $\partial_i W_{\text{ext}}(\mathbf{b}) = \partial_i[W_{\text{tot}}(\mathbf{b}) - W_{\text{trap}}(\mathbf{b})]$ and position $\mathbf{b}$ is obtained by back focal plane interferometry.[18,19]

The incident electric field $\mathbf{E}_{\text{in}}$ and the field scattered by the trapped probe $\mathbf{E}_{\text{pr}}$ interfere. In the back focal plane of the detection lens a quadrant photodiode (QPD) records the interference intensity $I_{\text{pr}}$, which depends on the phase difference $\Phi_{\text{in}}(k_x, k_y) - \Phi_{\text{pr}}(k_x, k_y, \mathbf{b}_{\text{pr}})$ between the two fields. The phase $\Phi_{\text{pr}}(k_x, k_y, \mathbf{b}_{\text{pr}})$ is linear to the position $\mathbf{b}_{\text{pr}}$ within the central region of the focus. The variables in the back focal plane are $k_x$ and $k_y$ with $k_\perp = (k_x^2 + k_y^2)^{1/2}$. To increase readability we will drop the dependencies on $k_x$, $k_y$, and $\mathbf{b}_{\text{pr}}$ after the first line:

$$I_{\text{pr}}(k_x, k_y, \mathbf{b}_{\text{pr}}) = |\mathbf{E}_{\text{in}}(k_x, k_y) + \mathbf{E}_{\text{pr}}(k_x, k_y, \mathbf{b}_{\text{pr}})|^2$$

$$= |\mathbf{E}_{\text{in}}|^2 + |\mathbf{E}_{\text{pr}}|^2 + |\mathbf{E}_{\text{in}}||\mathbf{E}_{\text{pr}}|$$

$$\times \cos(\Phi_{\text{in}} - \Phi_{\text{pr}}). \quad (2)$$

From this the four signals $S_n$ are obtained by integrating over the quadrant areas $A_n$ with $n = 1, 2, 3, 4$:

$$S_n(\mathbf{b}) = \iint_{A_n} I(k_x, k_y, \mathbf{b})\Theta(k_0 \text{NA}_{\text{det}} - k_\perp)dk_x dk_y. \quad (3)$$

In the standard case the intensity $I$ is defined by $I = I_{\text{pr}}$ as expressed in Eq. (2). $\Theta$ is the Heaviside step function and allows optical tuning of the linear region and the sensitivity of the position signals with the numerical aperture $\text{NA}_{\text{det}}$ of the detection lens.[20] Summing up the signals of two adjacent quadrants and taking the difference to the sum of the remaining quadrants, provides a signal that is proportional to the lateral directions of the trapped probe. The axial position $b_z$ is proportional to the sum of all four signals $S_n$ due to the Gouy phase shift.[18,19] Combining the three signals in Cartesian coordinates we define the signal vector $\mathbf{S}$ as

$$\mathbf{S}(\mathbf{b}) = (S_x, S_y, S_z) = \frac{(S_1 - S_2 + S_3 - S_4), (S_1 + S_2 - S_3 - S_4), (S_1 + S_2 + S_3 + S_4)}{S_0}. \quad (4)$$
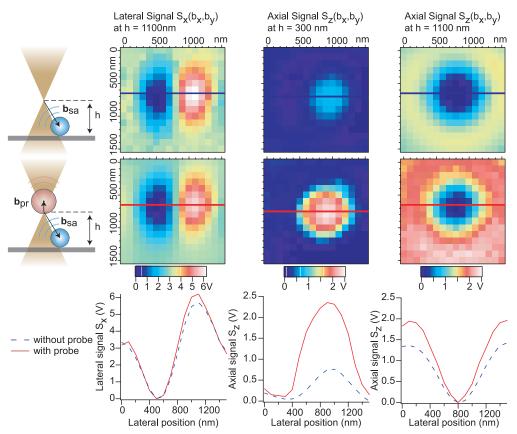
Fig. 2. (Color online) Detector signals $S_x$ and $S_z$ with and without trapped probe. The sample on the coverslip is a $D = 400$ nm silica sphere, the trapped probe is a $D = 535$ nm polystyrene sphere. The second column shows the lateral signal $S_x$. The third and fourth columns show the axial signal $S_z$ at a distance $h = 300$ nm and $h = 1100$ nm of the laser focus to the surface. Top row, lateral and axial detector signals of the sample on the coverslip at two different heights $h$; middle row, corresponding detector signals formed by both the sample and the trapped probe; bottom row, linescans from the graphs above.

$S_0$ is the intensity incident on the quadrant photodiode in the absence of the trapped probe.

The signal $\mathbf{S}(\mathbf{b}) = \hat{g}\mathbf{b} + \text{const}$ is linear to the deviation from the equilibrium position $\Delta\mathbf{b} = \mathbf{b} - \mathbf{b}_0$. The factor of proportionality, the so-called detection sensitivity, is given by the second order tensor $\hat{g}$. Near the equilibrium position[15] we can assume $\hat{g}$ to be in diagonal form, i.e., only entries $g_{ii}$ are nonzero. Furthermore we assume the entries of the tensor to be independent of the actual position $(b_x, b_y, b_z)$. This equals the linear independence and orthogonality of the position signals $S_x$, $S_y$, and $S_z$ in the region of interest. An additional offset $\mathbf{S}_{\text{off}} = \mathbf{S}(\mathbf{b} = 0)$ is subtracted electronically and plays no further role. Additional surface effects that alter the position signal are compiled into the term $\Delta\mathbf{S}_{\text{surf}\,i}(h)$. Its components and how to account for this additional term are discussed after Eq. (11). The signal is then given by

$$S_i(b_i) \approx g_{ii}(\Delta b_i + b_{0i}) + S_{\text{off}\,i} + \Delta S_{\text{surf}\,i}(h). \quad (5)$$

From this $\Delta b_i$ can be obtained as $\Delta b_i = g_{ii}^{-1}[S_i - g_{ii}b_{0i} - S_{\text{off}\,i} - \Delta S_{\text{surf}\,i}(h)]$. The force and potential acting on the probe are provided directly by $\Delta b_i$ as shown in Eq. (1).

Integration over the intensity in Eq. (3) can be exchanged with the subtraction and addition of signals (integrated intensities) in Eq. (4). Therefore we look at the intensities $I$ rather than at the signals $S$ in the following and get back to the signals later on.

The intensity $I(k_x, k_y, \mathbf{b})$ used in Eq. (3) can be defined depending on the configuration of sample and probe. If we consider the resulting intensity of a sample placed at $\mathbf{b}_{\text{sa}}$ without a probe being present, we write correspondingly to Eq. (2)

$$I_{\text{sa}}(k_x, k_y, \mathbf{b}_{\text{sa}}) = |\mathbf{E}_{\text{in}}|^2 + |\mathbf{E}_{\text{sa}}|^2 + |\mathbf{E}_{\text{in}}||\mathbf{E}_{\text{sa}}|$$
$$\times \cos(\Phi_{\text{in}} - \Phi_{\text{sa}}). \quad (6)$$

In the first row of Fig. 2 the resulting signals $S_x$ and $S_z$ are shown for a spherical sample made of silica with a diameter $D_{\text{sa}} = 400$ nm.

In the presence of a trapped probe (position $\mathbf{b}_{\text{pr}}$) above the sample (position $\mathbf{b}_{\text{sa}}$), not only the incident field $\mathbf{E}_{\text{in}}$, but also the scattered field $\mathbf{E}_{\text{sa}}$ is scattered at the probe. Here, multiple scattering between probe and sample will not be considered in the total intensity $I_{\text{tot}}$. Again, we will drop the dependencies on $k_x, k_y, \mathbf{b}_{\text{sa}}$, and $\mathbf{b}_{\text{pr}}$ after the second line to increase readability:

$$\begin{aligned}
I_{\text{tot}}(k_x, k_y, \mathbf{b}_{\text{sa}}, \mathbf{b}_{\text{pr}}) &= |\mathbf{E}_{\text{tot}}(k_x, k_y, \mathbf{b}_{\text{sa}}, \mathbf{b}_{\text{pr}})|^2 \\
&= |\mathbf{E}_{\text{in}}(k_x, k_y) + \mathbf{E}_{\text{sa}}(k_x, k_y, \mathbf{b}_{\text{sa}}) \\
&\quad + \mathbf{E}_{\text{pr}}(k_x, k_y, \mathbf{b}_{\text{sa}}, \mathbf{b}_{\text{pr}})|^2 \\
&= |\mathbf{E}_{\text{in}}|^2 + |\mathbf{E}_{\text{sa}}|^2 + |\mathbf{E}_{\text{pr}}|^2 \\
&\quad + |\mathbf{E}_{\text{in}}||\mathbf{E}_{\text{sa}}| \cos(\Phi_{\text{in}} - \Phi_{\text{sa}}) \\
&\quad + |\mathbf{E}_{\text{in}}||\mathbf{E}_{\text{pr}}| \cos(\Phi_{\text{in}} - \Phi_{\text{pr}}') \\
&\quad + |\mathbf{E}_{\text{sa}}||\mathbf{E}_{\text{pr}}| \cos(\Phi_{\text{sa}} - \Phi_{\text{pr}}').
\end{aligned} \tag{7}$$

In this case the field scattered at the probe $\mathbf{E}_{\text{pr}} = \mathbf{E}_{\text{pr}}(\mathbf{b}_{\text{pr}}, \mathbf{b}_{\text{sa}})$ depends on the positions of the sample and the probe itself. To indicate this dependence on the phase, we write $\Phi_{\text{pr}}' = \Phi_{\text{pr}}'(\mathbf{b}_{\text{sa}}, \mathbf{b}_{\text{pr}})$ in contrast to the unprimed phase $\Phi_{\text{pr}} = \Phi_{\text{pr}}(\mathbf{b}_{\text{pr}})$ in Eq. (2). The resulting signals are shown in the second row of Fig. 2 for a trapped probe with $r_{\text{pr}} = 267$ nm. The additional scattering at the sample [additional terms in Eq. (7) containing $\mathbf{E}_{\text{sa}}$] tampers the probe's position signal although the probe's position remains unchanged at a distance of $h > D_{\text{sa}} + r_{\text{pr}}$, which is shown in the fourth column of Fig. 2 measured at a distance of $h = 1100$ nm to the surface. To obtain the correct position in the presence of the disturbance induced by the sample, we apply the following first-order phase correction: we subtract the intensity generated only by the sample $I_{\text{sa}}(k_x, k_y, \mathbf{b}_{\text{sa}})$ from the intensity resulting from sample and probe $I_{\text{tot}}(k_x, k_y, \mathbf{b}_{\text{sa}}, \mathbf{b}_{\text{pr}})$. We get

$$\begin{aligned}
I_{\text{diff}} = I_{\text{tot}} - I_{\text{sa}} &= |\mathbf{E}_{\text{pr}}|^2 + |\mathbf{E}_{\text{in}}||\mathbf{E}_{\text{pr}}|\cos(\Phi_{\text{in}} - \Phi_{\text{pr}}') \\
&\quad + |\mathbf{E}_{\text{sa}}||\mathbf{E}_{\text{pr}}|\cos(\Phi_{\text{sa}} - \Phi_{\text{pr}}'),
\end{aligned} \tag{8}$$

with $\mathbf{E}_{\text{pr}} = \mathbf{E}_{\text{pr}}(\mathbf{b}_{\text{pr}}, \mathbf{b}_{\text{sa}})$. We assume that the influence of the sample on the signal is present, but small. In this case we can drop the dependency of the scattered field $\mathbf{E}_{\text{pr}}$ on the position of the sample $\mathbf{b}_{\text{sa}}$, such that $\mathbf{E}_{\text{pr}}(\mathbf{b}_{\text{pr}}, \mathbf{b}_{\text{sa}}) \approx \mathbf{E}_{\text{pr}}(\mathbf{b}_{\text{pr}})$ and $\Phi_{\text{pr}}' \approx \Phi_{\text{pr}}$. A small scattered field $\mathbf{E}_{\text{sa}}$ also satisfies

$$\begin{aligned}
|\mathbf{E}_{\text{sa}}||\mathbf{E}_{\text{pr}}|\cos(\Phi_{\text{sa}} - \Phi_{\text{pr}}') &\ll |\mathbf{E}_{\text{in}}|^2, \\
|\mathbf{E}_{\text{sa}}||\mathbf{E}_{\text{pr}}|\cos(\Phi_{\text{sa}} - \Phi_{\text{pr}}') &\ll |\mathbf{E}_{\text{pr}}|^2.
\end{aligned} \tag{9}$$

With these two assumptions, the comparison of Eqs. (2) and (8) leads to the following expression, which is the central result of this paper:

$$I_{\text{pr}} \approx I_{\text{tot}} - I_{\text{sa}} + |\mathbf{E}_{\text{in}}|^2. \tag{10}$$

To apply the aforementioned correction we need to consider the actual position of the probe $\mathbf{b}_{\text{pr}}$. After integration of approximation (10) we get

$$\mathbf{S}_{\text{pr}}(\mathbf{b}_{\text{pr}}) - S_0 \approx S_{\text{diff}}(\mathbf{b}_{\text{pr}}) = \mathbf{S}_{\text{tot}}(\mathbf{b}_{\text{pr}}) - \mathbf{S}_{\text{sa}}(\mathbf{b}_{\text{pr}}). \tag{11}$$

In contrast to $\mathbf{S}_{\text{tot}}(\mathbf{b}_{\text{pr}})$ the measured position signal of the probe $\mathbf{S}_{\text{tot}}(\mathbf{b}_{\text{pr}}')$ contains the term $\Delta\mathbf{S}_{\text{surf}}$, which has its origin in the probe's repulsion from the surface (steric interaction) and a standing wave between the surface and the trapped particle.[21,22] In Fig. 3
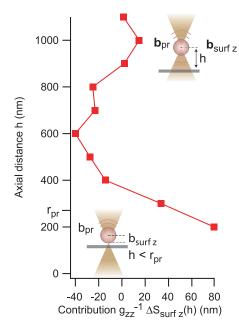


Fig. 3. (Color online) Deviation from the center position due to surface effects plotted against the distance to the surface $h$. The contribution of the surface to the signal $\Delta S_{\text{surf}\,z}(h)$ increases linear close to the surface ($< D_{\text{pr}}/2 = r_{\text{pr}}$).

$\Delta S_{\text{surf}\,z}(h) = S_{\text{pr}\,z}(b_z) - S_{\text{off}\,z}$ is shown along the axial direction without the influence of the sample from the surface. The steric repulsion from the surface leads to a constraint of the particle's diffusion volume and therefore to a shift of the average position signal. This shift $\Delta S_{\text{surf}\,z}(h)$ is linear for distances $h$ comparable to the axial extension of the optical trap as shown in Fig. 3. For distances $h$ exceeding the diffusion volume, the contribution from the standing wave is dominant, which results from the reflection between the probe and the surface. The amplitude of the standing wave fades to zero at a distance of several micrometers. Far away from the surface we get $\Delta\mathbf{S}_{\text{surf}}(h) = 0$. Both effects act only on the axial signal, the lateral components of $\Delta\mathbf{S}_{\text{surf}}(h)$ are zero. To compensate for these effects, we subtract the measurable signal $\Delta\mathbf{S}_{\text{surf}}(h)$ from the measured position signal of the probe $\mathbf{S}_{\text{tot}}(\mathbf{b}_{\text{pr}}')$:

$$\begin{aligned}
\mathbf{S}_{\text{tot}}(\mathbf{b}_{\text{pr}}) &= \mathbf{S}_{\text{tot}}(\mathbf{b}_{\text{pr}}') - \Delta\mathbf{S}_{\text{surf}}(h) \\
&= \hat{g}_{\text{tot}}(\Delta\mathbf{b} + \mathbf{b}_0) + \mathbf{S}_{\text{off tot}}.
\end{aligned} \tag{12}$$

Correspondingly, and also for small $\Delta\mathbf{b}$, the measured signal from the sample is linear to the displacement $\Delta\mathbf{b}$:

$$\mathbf{S}_{\text{sa}}(\mathbf{b}_{\text{pr}}) = \hat{g}_{\text{sa}}(\Delta\mathbf{b} + \mathbf{b}_0) + \mathbf{S}_{\text{off sa}}, \tag{13}$$

where $\hat{g}_{\text{pr}} \approx \hat{g}_{\text{diff}} = \hat{g}_{\text{tot}} - \hat{g}_{\text{sa}}$ and $\mathbf{S}_{\text{off diff}} = \mathbf{S}_{\text{off tot}} - \mathbf{S}_{\text{off sa}}$. By inserting Eqs. (12) and (13) into Eq. (11) and solving for $\Delta\mathbf{b}$ we obtain the displacement

$$\Delta\mathbf{b} = \hat{g}_{\text{diff}}^{-1}[\mathbf{S}_{\text{diff}}(\mathbf{b}_{\text{pr}}) - \mathbf{S}_{\text{off diff}}] - \mathbf{b}_0. \tag{14}$$

The constant terms $\hat{g}_{\text{diff}}^{-1}\mathbf{S}_{\text{off diff}}$ and $\mathbf{b}_0$ are not considered further as they represent only a constant shift of

the signal and therefore contain no information in the lateral and axial directions.

The problem is that only $\mathbf{S}_{sa}(\mathbf{b}_0)$ is known, but not the $\mathbf{S}_{sa}(\mathbf{b}_{pr})$ used in Eq. (11). However, the missing information, the displacement of the probe $\Delta\mathbf{b}$, can be obtained iteratively. Starting with order $n = 0$ and $\Delta\mathbf{b}^0 = 0$, we apply the following correction scheme repeatedly: first, we build the difference signal $\mathbf{S}_{diff}(\mathbf{b}_0 + \Delta\mathbf{b}^{n+1})$ of the next order according to

$$\mathbf{S}_{diff}(\Delta\mathbf{b}^{n+1} + \mathbf{b}_0) = \mathbf{S}_{tot}(\mathbf{b}_{pr}) - \mathbf{S}_{sa}(\Delta\mathbf{b}^n + \mathbf{b}_0). \quad (15)$$

From this we are able to calculate a refined value for the displacement $\Delta\mathbf{b}^{n+1}$:

$$\Delta\mathbf{b}^{n+1} = \hat{g}_{diff}^{-1}[\mathbf{S}_{diff}(\Delta\mathbf{b}^{n+1} + \mathbf{b}_0)]. \quad (16)$$

By putting $\Delta\mathbf{b}^{n+1}$ back into Eq. (15) and repeating the procedure, we can iteratively determine $\Delta\mathbf{b}$. Typically with $n < 10$, $\Delta\mathbf{b}^n$ converges to $\Delta\mathbf{b}$, i.e., $\Delta\mathbf{b}^n \approx \Delta\mathbf{b}$.

### 3. Experimental Results

That approximation (10) could correct the tracking signal of a probe for phase disturbances by a sample was proved experimentally. As a sample we used a spherical silica particle (bead) with a diameter $D_{sa} = 400$ nm from Bangs Laboratories, Incorporated with a specified index of refraction $n_{pr} = 1.43$ to $1.46$ at a wavelength of $\lambda = 589$ nm. The beads in solution were dried on a coverslip made of borosilicate glass to produce a sparsely covered surface. The probes, polystyrene particles with diameters $D_{pr} = 356$ and 535 nm, were trapped with a strongly focused laser beam (water-immersion lens IR corrected, NA of 1.2, Olympus, Japan) at a wavelength of $\lambda_0 = 1064$ nm. The probes were trapped 100–150 nm behind the geometric focus. A complete description of the setup used is given in Ref. 18.

The idea behind the experiment is to move the probe with the optical trap over a flat surface with the sample. The position of the probe can be measured correctly only by considering the phase disturbance of the sample. While the probe and sample are not in contact, no interaction takes place and the probe's position is expected to move along with the optical trap. When the probe and sample contact each other, the probe is displaced by steric interaction. The expected displacement $\Delta b_z$ ($\gg \Delta b_{x,y}$ since $\kappa_{x,y} \gg \kappa_z$) corresponds to a segment of a circle with radius $R = (D_{pr} + D_{sa})/2$, i.e., $\Delta b_z = [R^2 - (b_{0x} - b_{sax})^2]^{1/2} + D_{pr}/2$, $\Delta b_z \geq 0$.

Before the surface scans were performed, the trap and the detector were calibrated by tracking the probe inside the trap for $T = 10$ s at a distance of $h \approx 10$ μm. From this measurement the proportionality factors $g_{ii}$ were determined by using the Langevin method.[18] The laser focus was scanned with a trapped probe and without a probe immediately after each other to minimize the drifts of laser power and coverslip position. The scan speed was sufficiently slow to allow a relaxation of the probe to the position $\mathbf{b}_0$ inside the trap. If the resting time at each mea-
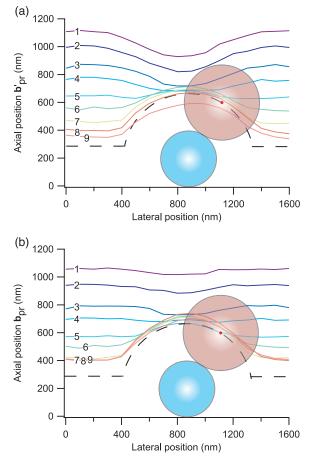


Fig. 4. (Color online) Probe (in red) is rolled over the spherical surface structure (in blue) by the optical trap. (a) Measured traces of a $D = 535$ nm polystyrene sphere scanned over a $D = 400$ nm silica sphere. (b) Corrected particle traces. The colored and numbered traces represent the probe's center position at different heights above the surface.

suring point was comparable to the autocorrelation time $\tau$, the probe would be dragged along the scan direction, resulting in an asymmetric displacement trace by the spherical sample.

Figure 2 shows the signal distributions in the $xy$ plane. The lateral signal $S_x$ is almost unaffected by the probe (second column). In the axial direction at the same distance $h = 1100$ nm, the two signals are still in reasonable agreement (fourth column). Close to the surface, ($h = 300$ nm) the axial signal is amplified by the presence of the probe (third column). In Fig. 4 the traces $\Delta\mathbf{b}(t) + \mathbf{b}_0$ of the trapped probe with $D_{pr} = 535$ nm are shown without and with phase correction at different heights $h$. The dashed line in both Figs. 4(a) and 4(b) marks the theoretical trace closest to the surface assuming the probe is in continuous contact with the surface and sample. One possible configuration of the two spheres is shown schematically. The scans were performed with a step width of 100 nm in the lateral and axial directions. At each point data were acquired for $T = 100$ ms at a rate of $f = 1$ kHz. The average of 100 measurements per point was saved for later processing.
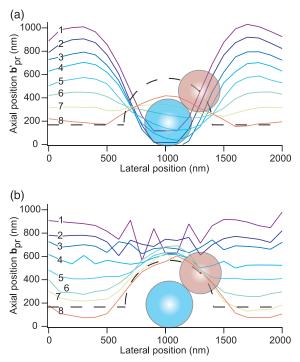
Fig. 5. (Color online) Probe (in red) is rolled over the spherical surface structure (in blue) by the optical trap. (a) Measured traces of a $D = 356$ nm polystyrene sphere scanned over a $D = 400$ nm silica sphere. (b) Corrected particle traces. The colored and numbered traces represent the probe's center position at different heights above the surface.

Figure 4(a) shows the measured traces of the probe without correction. Traces 1, 2, and 3 have pronounced dents toward the surface pretending a probe displacement of approximately $\Delta b_z = 200$ nm above the sample, whereas trace 9 would require the two spheres to penetrate each other. These artifacts are a result from the additional scattering of the sample underneath. After applying the corrections for surface effects and phase disturbances described in Section 2 we obtain the position traces shown in Fig. 4(b). The dents toward the surface have almost vanished resulting in the expected straight lines of traces 1–4 ($\Delta b = 0$). As the distance between the centers of the probe and the sample becomes smaller than $d \leq (535 \text{ nm} + 400 \text{ nm})/2 = 467$ nm, the probe in the trap is deflected by $\Delta b$ and the two spheres roll over each other. The fluctuations of the traces located close to the surface (7–9) are due to the extent of the optical trap and the averaging in the measurement process. The deviation of the latter traces from the theoretical dashed line is not fully understood. It is possible that the surface still exhibits a small electrostatic repulsion. It is more likely that the contribution of the standing wave is more complex and makes the correction less effective in the border area. This can also explain why trace 8 in Fig. 5(b) is below the theoretical dashed line.

Data measured with the smaller probe with $D_{pr} = 356$ nm are shown in Fig. 5. Instead of smooth dents as in the former case, Fig. 5(a) reveals extreme
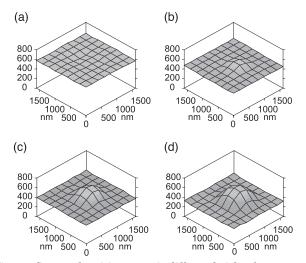


Fig. 6. Corrected position traces in different heights for a trapped $D = 535$ nm polystyrene particle scanned over a $D = 400$ nm silica particle. Height $h$ above the coverslip (a) 600 nm, (b) 500 nm, (c) 400 nm, (d) 300 nm. With decreasing height, the position of the trapped particle reveals the underlying structure.

dips pretending a displacement $\Delta b_z \approx 800$ nm. These are due to the phase disturbance that produces a phase shift comparable to that stemming from the probe. Close to the surface the signal progression flips as can be seen with trace 8. After applying the corrections, the traces are in reasonable agreement with the expected rollover trajectory in Fig. 5(b), drawn as a dashed line. The noisy behavior particularly visible in traces 1 and 2 have their origin in the limited extent of data available to the iterative correction. Increasing the axial scan area will reduce this artifact.

The validity of the approximation given in expressions (9) can be checked by comparing the relative magnitudes of the fields $|\mathbf{E}|$. The fields are related to the scattering efficiency $Q_{sca}$ by $|\mathbf{E}| \propto r(Q_{sca})^{1/2}$ for small spheres with radius $r$. Values for the scattering efficencies are taken from Rohrbach.[23] For the sample used, the scattering efficency has a value of $Q_{sca\,sa} = 0.018$. The probes consisting of polystyrene with $n_{pr} = 1.57$ have scattering efficiencies $Q_{sca\,pr} = 0.22$ for the $D = 535$ nm sphere and $Q_{sca\,pr} = 0.08$ for the $D = 356$ nm sphere. The ratio $|\mathbf{E}_{pr}|^2/(|\mathbf{E}_{sa}||\mathbf{E}_{pr}|)$ in expressions (9) with $\cos(\Phi_{sa} - \Phi_{pr}') = 1$ has a value of 4.6 for the $D = 535$ nm sphere. For the sphere with $D = 356$ nm, the ratio decreased to 1.9. From this it follows, that the "much less than" requirement in expressions (9) is relaxed.

To demonstrate that our method works in all dimensions (the 3D functionality), Fig. 6 shows selected slices parallel to the surface of four different heights. Data are taken from the same measurement as shown in Fig. 4. From these slices the rotational symmetry of the underlying sample is clearly visible as the height to the surface is reduced going from Figs. 6(a) to 6(d). The black grid indicates every second data point.

## 4. Conclusion

We have presented a procedure to correct for phase disturbances introduced by surface structures on the tracking signal of an optically trapped probe. The theoretical framework for the correction was derived. By using a simple configuration with a sphere as a well-defined surface structure we showed the experimental applicability of the correction. The experimental results confirm the efficiency of the correction scheme, the measured particle trajectories were recovered in good agreement with the expected trajectories. No specific assumptions about the phase disturbance were made, allowing the correction to be applied to arbitrarily shaped scatterers with phase shifts comparable to that of the probe. We believe that this scheme will find broad application in optical trapping and scanning coherence microscopy.

## References

1. G. Binnig, C. F. Quate, and C. Gerber, "Atomic force microscope," Phys. Rev. Lett. **56,** 930–933 (1986).
2. B.-W. Yang and H.-P. D. Shieh, "Interlayer cross talk in dual-layer read-only optical disks," Appl. Opt. **38,** 333–338 (1999).
3. F. Roddier, ed., *Adaptive Optics in Astronomy* (Cambridge U. Press, 2004).
4. M. Feierabend, M. Rückel, and W. Denk, "Coherence-gated wave-front sensing in strongly scattering samples," Opt. Lett. **29,** 2255–2257 (2004).
5. C. J. R. Sheppard, M. Roy, and M. D. Sharma, "Image formation in low-coherence and confocal interference microscopes," Appl. Opt. **43,** 1493–502 (2004).
6. M. G. L. Gustafsson, "Nonlinear structured-illumination microscopy: wide-field fluorescence imaging with theoretically unlimited resolution," Proc. Natl. Acad. Sci. U.S.A. **102,** 13,081–13,086 (2005).
7. C. Bustamante, Z. Bryant, and S. B. Smith, "Ten years of tension: single-molecule DNA mechanics," Nature **421,** 423–427 (2003).
8. M. W. Allersma, F. Gittes, M. J. deCastro, R. J. Stewart, and C. F. Schmidt, "Two-dimensional tracking of ncd motility by back focal plane interferometry," Biophys. J. **74,** 1074–1085 (1998).
9. L. P. Ghislain and W. W. Webb, "Scanning-force microscope based on an optical trap," Opt. Lett. **18,** 1678–1680 (1993).
10. H. Hertz, L. Malmqvist, L. Rosengren, and K. Ljungberg, "Optically trapped nonlinear particles as probes for scanning near-field optical microscopy," Ultramicroscopy **57,** 309–312 (1995).
11. S. Kawata, Y. Inouye, and T. Sugiura, "Near-field scanning optical microscope with a laser trapped probe," Jpn. J. Appl. Phys. **33,** L1725–L1727 (1994).
12. E. L. Florin, A. Pralle, J. K. Hörber, and E. H. Stelzer, "Photonic force microscope based on optical tweezers and two-photon excitation for biological applications," J. Struct. Biol. **119,** 202–11 (1997).
13. G. M. Whitesides, J. K. Kriebel, and J. C. Love, "Molecular engineering of surfaces using self-assembled monolayers," Sci. Prog. **88,** 17–48 (2005).
14. J. Groll, K. Albrecht, P. Gasteier, S. Riethmueller, U. Ziener, and M. Moeller, "Nanostructured ordering of fluorescent markers and single proteins on substrates," ChemBioChem **6,** 1782–7 (2005).
15. H. Kress, E. H. K. Stelzer, G. Griffiths, and A. Rohrbach, "Control of relative radiation pressure in optical traps: application to phagocytic membrane binding studies," Phys. Rev. E **71,** 061927 (2005).
16. A. Pralle, P. Keller, E. L. Florin, K. Simons, and J. K. Hörber, "Sphingolipid-cholesterol rafts diffuse as small entities in the plasma membrane of mammalian cells," J. Cell Biol. **148,** 997–1008 (2000).
17. N. B. Becker, S. M. Altmann, T. Scholz, J. K. H. Hörber, E. H. K. Stelzer, and A. Rohrbach, "Three-dimensional bead position histograms reveal single-molecule nanomechanics," Phys. Rev. E **71,** 021907 (2005).
18. A. Rohrbach, C. Tischer, D. Neumayer, E.-L. Florin, and E. H. K. Stelzer, "Trapping and tracking a local probe with a photonic force microscope," Rev. Sci. Instrum. **75,** 2197–2210 (2004).
19. A. Pralle, M. Prummer, E. L. Florin, E. H. Stelzer, and J. K. Hörber, "Three- dimensional high-resolution particle tracking for optical tweezers by forward scattered light," Microsc. Res. Tech. **44,** 378–86 (1999).
20. A. Rohrbach, H. Kress, and E. H. K. Stelzer, "Three-dimensional tracking of small spheres in focused laser beams: influence of the detection angular aperture," Opt. Lett. **28,** 411–413 (2003).
21. A. Jonáš, P. Zemánek, and E.-L. Florin, "Single-beam trapping in front of reflective surfaces," Opt. Lett. **26,** 1466–1468 (2001).
22. K. C. Neuman and S. M. Block, "Optical trapping," Rev. Sci. Instrum. **75,** 2787–2809 (2004).
23. A. Rohrbach and E. H. K. Stelzer, "Optical trapping of dielectric particles in arbitrary fields," J. Opt. Soc. Am. A **18,** 839–853 (2001).